Supporting Information

Effects of Carbon Defects on Interfacial Anchoring of NiFe-LDH for Seawater Electro-oxidation

Heng Xu,[a] Shi-Jun Xie,[b] Chao Lv,[b] Jun-Tao Li,[b] Yao Zhou,[*b] Shi-Gang Sun[*a]

[a] College of Chemistry and Chemical Engineering, Xiamen University, Xiamen 361005, China
[b] College of Energy, Xiamen University, Xiamen 361005, China.
E-mail: sgsun@xmu.edu.cn; zhouy@xmu.edu.cn

Table S1. Calculated integrated area ratio I_D/I_G from the Raman spectrum of the four CFD_r samples.

CFD_r	**Sample**	***r* (I_D/I_G)**	
		intensity ratio	**average**
$CFD_{0.11}$	1	0.13	0.11±0.02
	2	0.11	
	3	0.09	
$CFD_{0.26}$	1	0.21	0.26±0.03
	2	0.29	
	3	0.27	
$CFD_{0.42}$	1	0.38	0.42±0.03
	2	0.46	
	3	0.41	
$CFD_{0.51}$	1	0.53	0.51±0.02
	2	0.47	
	3	0.52	

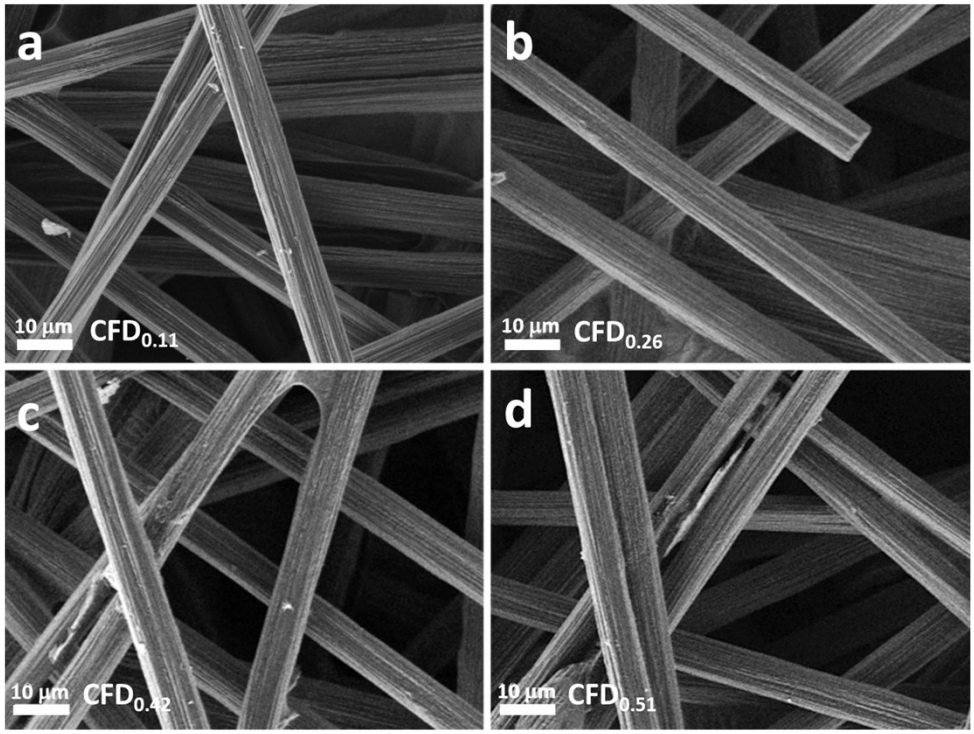

Figure. S1. SEM images of the four CFD_r samples.

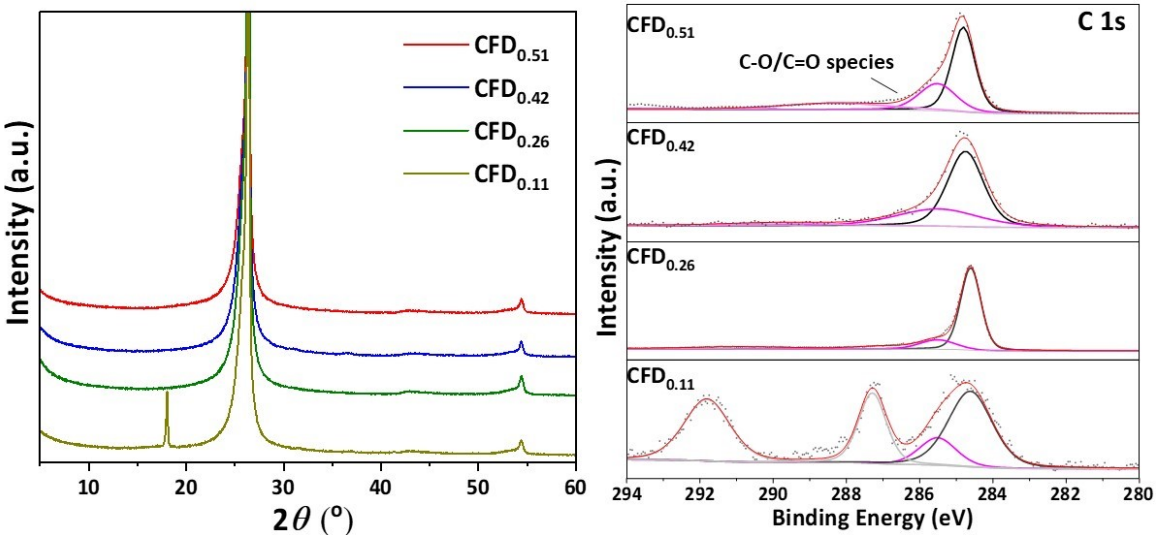

Figure S2. (Left) XRD patterns and (Right) C 1s XPS of the four bare CFD_r. Note that the pristine commercial sample $CFD_{0.11}$ demonstrates a peak at around 18.0° in the XRD pattern and the two additional peaks at higher binding energy in its XPS spectrum, which is assigned to the PTFE coating.

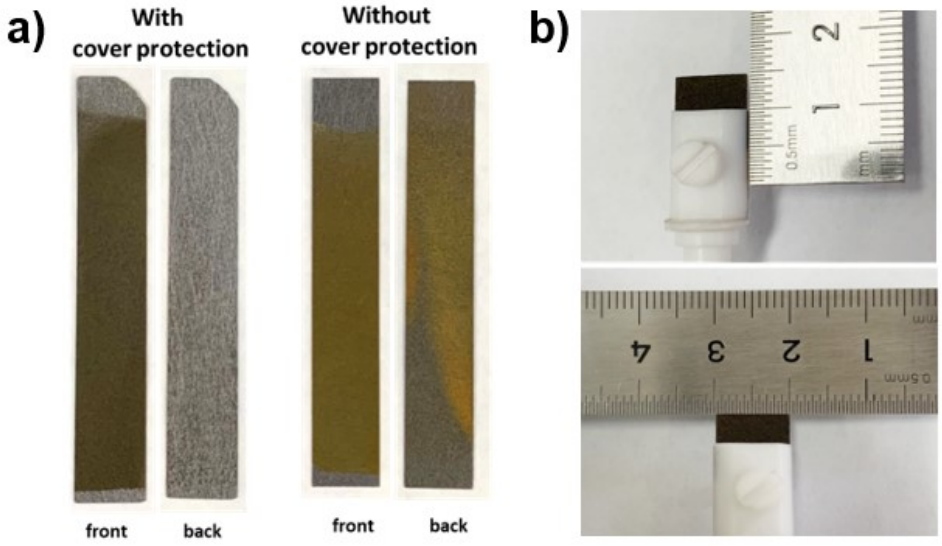

Figure S3. Optical photographs of a) controlled homogenous growth of binder-free NiFe-LDH on defective carbon fabrics with and without one side of the carbon fabric being covered. b) working electrode with exact 0.5 × 1.0 cm carbon fabric.

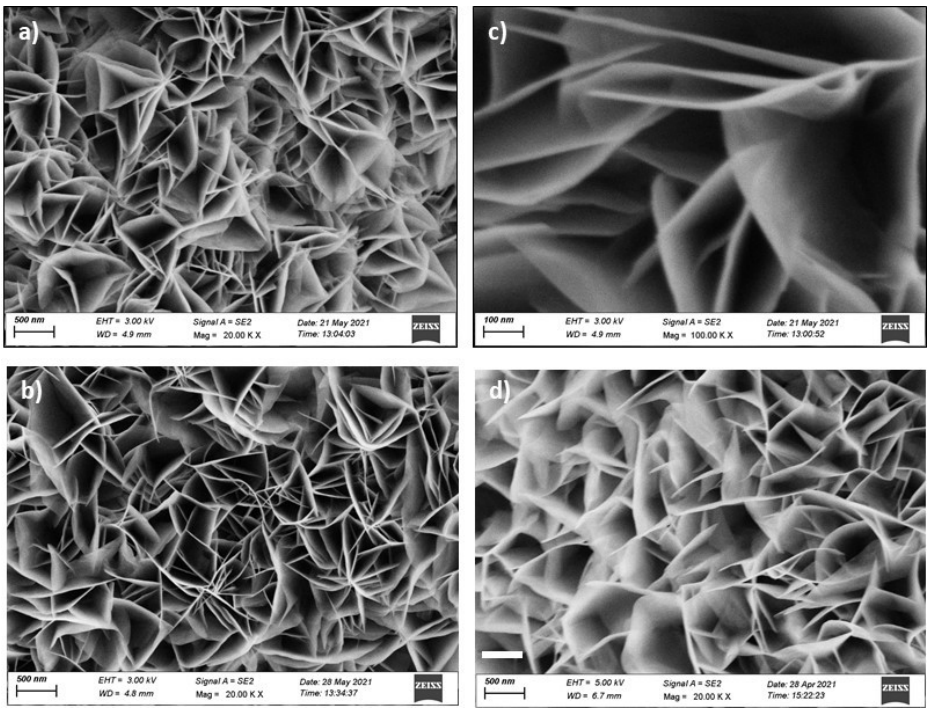

Figure S4. SEM images of a) NiFe/$CFD_{0.11}$, b) NiFe/$CFD_{0.26}$, c) NiFe/$CFD_{0.42}$, and d) NiFe/$CFD_{0.51}$ All the NiFe-LDHs on-site grown on the defected carbon have similar staggered homogenous arrays with thin sheets of 12-13 nm thickness.

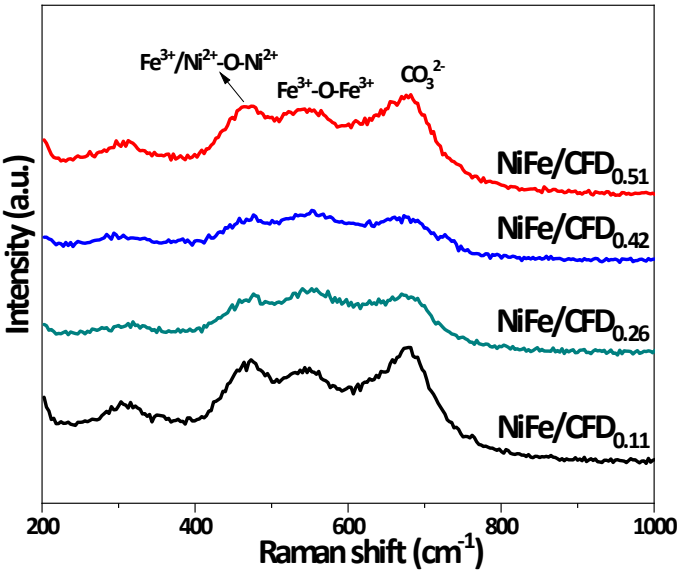

Figure S5. Raman spectroscopy of the binder-free NiFe-LDH/carbon fabric electrodes (NiFe/CFD$_r$). The representative shifts around 460 and 550 cm^{-1} are characteristic of Fe^{3+}/Ni^{2+}–O–Ni^{2+} and Fe^{3+}–O–Fe^{3+} bonds while the shift around 690 cm^{-1} is attributed to the productive intercalation of carbonate anions.

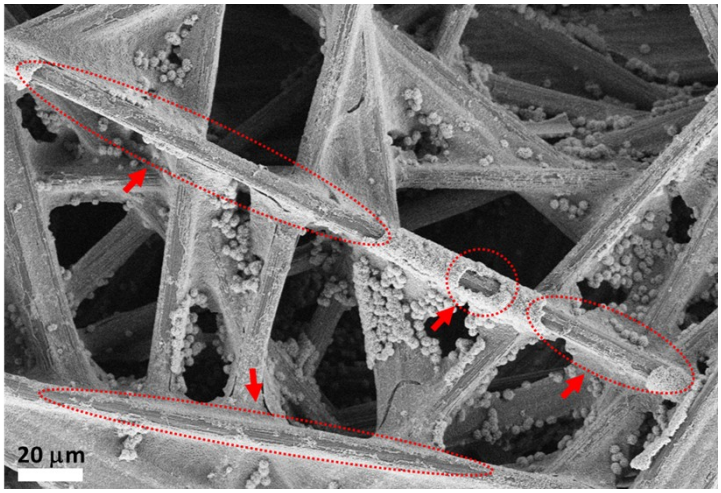

Figure S6. SEM image of the spent NiFe/CFD$_{0.11}$ sampled at the point marked by the red circle shown in Fig.5a in the main text.

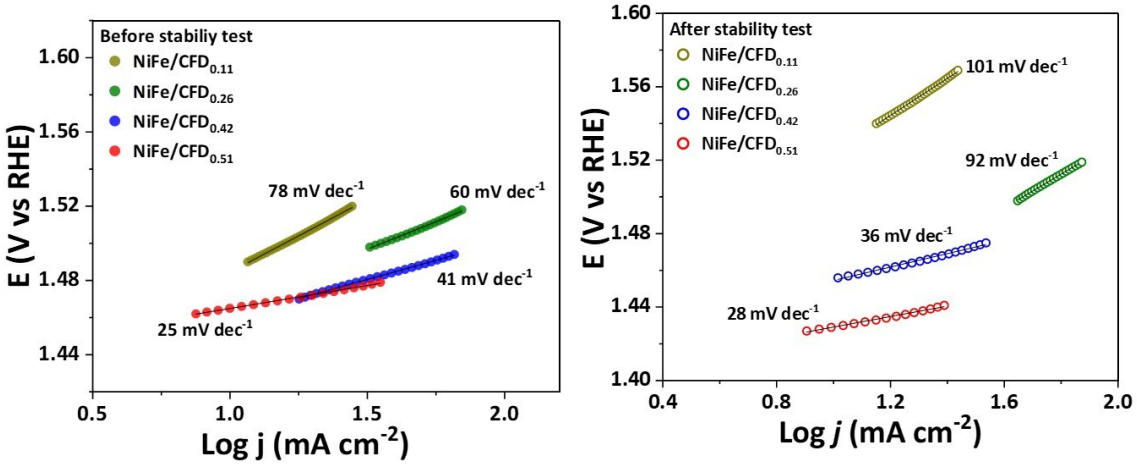

Figure S7. Tafel slopes of the NiFe-LDH array coated electrodes (left) before and (right) after the short-term stability test in 1M KOH + 2M NaCl for 160 h.

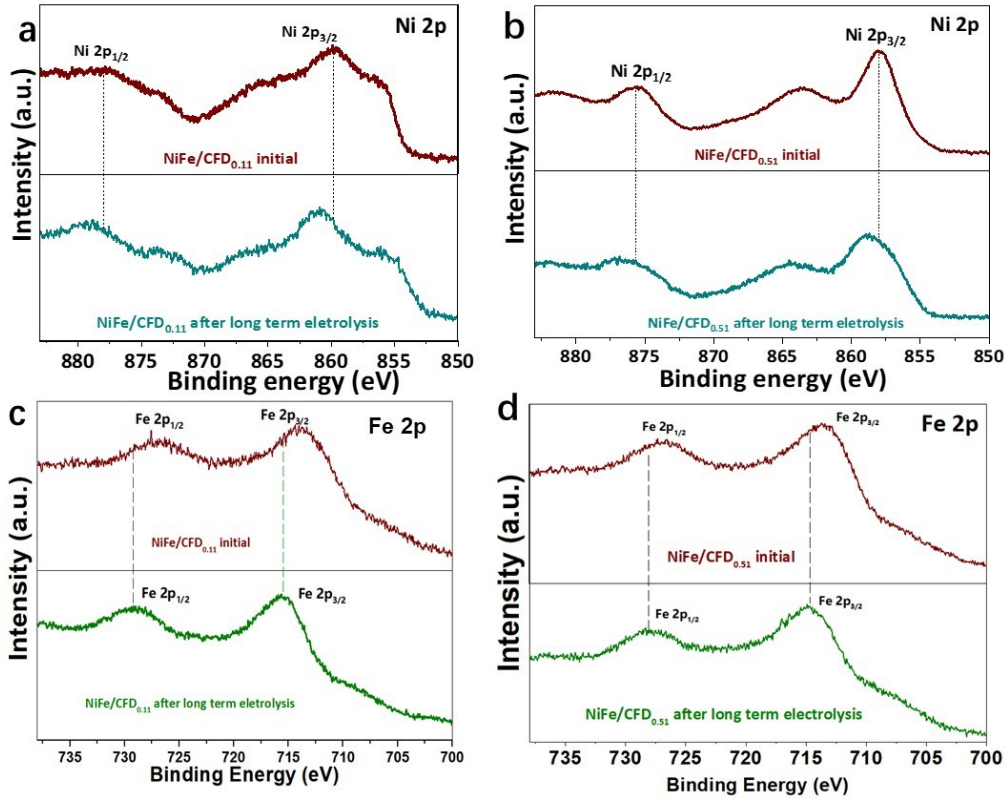

Figure S8. (a,b) Ni 2p and (c,d) Fe 2p XPS spectra in the (a,c) NiFe/$CFD_{0.11}$ and (b,d) NiFe/$CFD_{0.51}$ before and after the stability test.

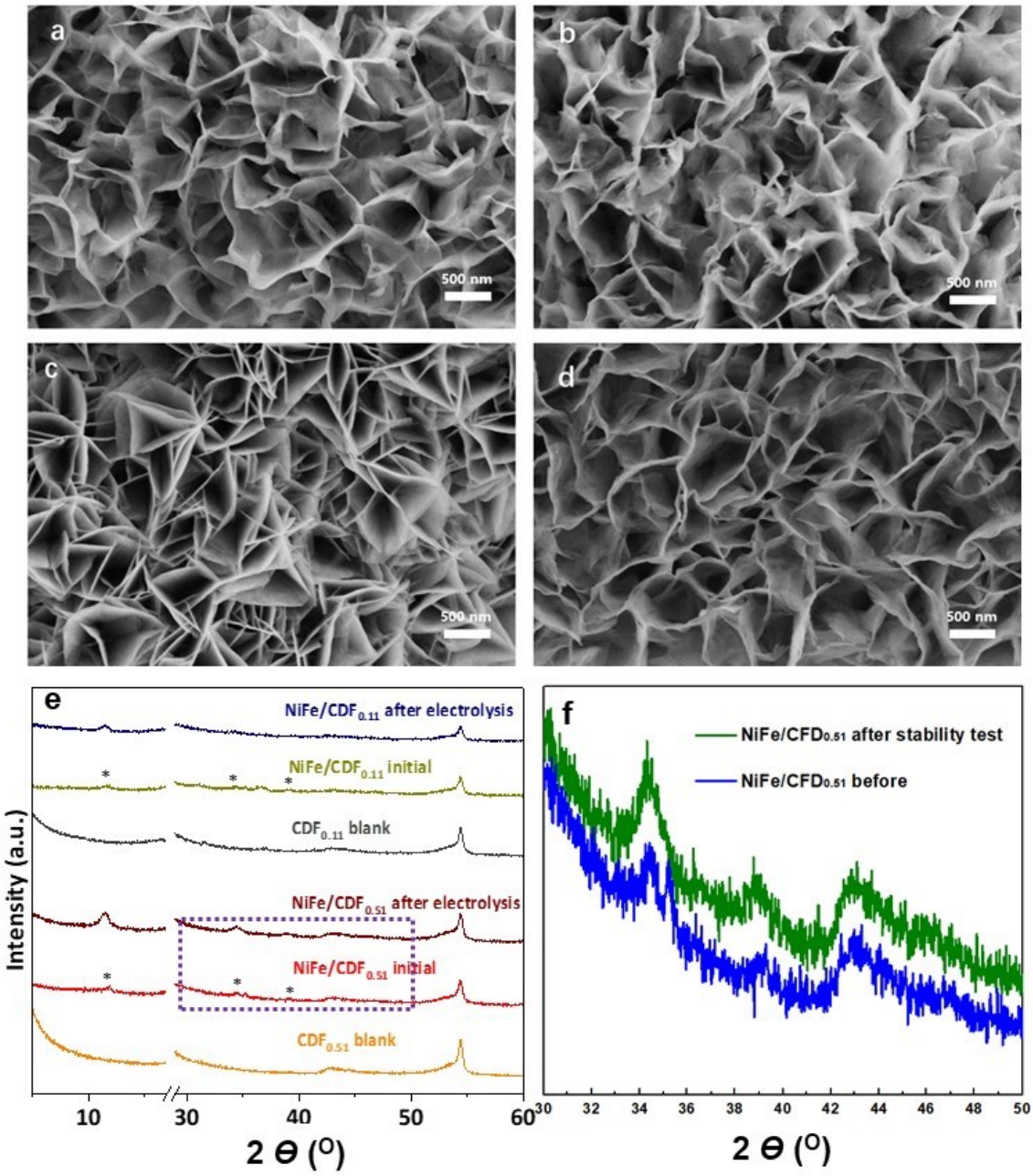

Figure S9. SEM images of NiFe/$CDF_{0.11}$ (a) before and (b) after the long-term electrolysis; SEM images of NiFe/$CDF_{0.51}$ (c) before and (d) after the long-term electrolysis; (e) Comparison of the XRD patterns of the blank CDF and the NiFe/$CDF_{0.51}$ and NiFe/$CDF_{0.11}$ before and after the stability tests;(f) Enlarged XRD patterns framed in (e). Note that the CDF has strong XRD peaks owing to the PTFE coating, as a result of which the peaks of NiFe-LDH look weak apparently.

Table S2. Performance comparison of different NiFe-based electrocatalysts supported on

various carbonaceous substrates.

Composite electrodes	**Overpotential (mV) @10mV cm^{-2}**	**Tafel slope (mV dec^{-1})**	**Stability**	**Test condition @$\eta_{\text{mA cm-2}}$**	**Ref.**
NiFe/CDF$_{0.51}$	233	25	550 h	1 M KOH + seawater @η_{500}	This work
NiFe/CDF$_{0.42}$	236	41	160 h	1 M KOH + saline @η_{200}	This work
NiFe/CDF$_{0.26}$	240	60	160 h	1 M KOH + saline @η_{200}	This work
NiFe/CDF$_{0.11}$	253	78	12 h	1 M KOH + saline @η_{150}	This work
$Ni_{2/3}Fe_{1/3}$-GO	230	42	10 h	1 M KOH @η_{10}	[1]
NiCoPS/CC	230	62.3	40 h	1 M KOH @η_{10}	[2]
$Co_{0.8}Fe_{0.2}$OOH@C/CFP	254	46	360 h	1 M KOH @η_{100}	[3]
$CoNi_xS_y$/NCP	278	71	10 h	0.1 M KOH @η_{13}	[4]
Ni_2Fe-SDS-LDH/CFP	289	39	10h	1 M KOH @η_{10}	[5]
NiS_2-Ni(OH)$_2$/CNT	290	110	70 h	1 M KOH @η_{10}	[6]
NCFPO/C@CC	300	53	100 h	1 M KOH + saline @η_{50}	[7]
NiFe-LDH/Co,N-CNF	312	60	80 h	6 M KOH @η_{25}	[8]
AC-NiO	320	49	10 h	1 M KOH @η_{10}	[9]
Ni/NiO/N-doped AC	346	70	30 h	0.1 M KOH @η_{30}	[10]
MHCM-z-BCC	350	-	100 h	buffered seawater @η_{14}	[11]

CNT, carbon nanotubes; CFP, carbon fiber paper; CNF, codoped carbon nanoframes; GO, graphene oxide; NCP, N-enriched porous carbon polyhedron; CC, carbon cloth; AC, activated carbon.

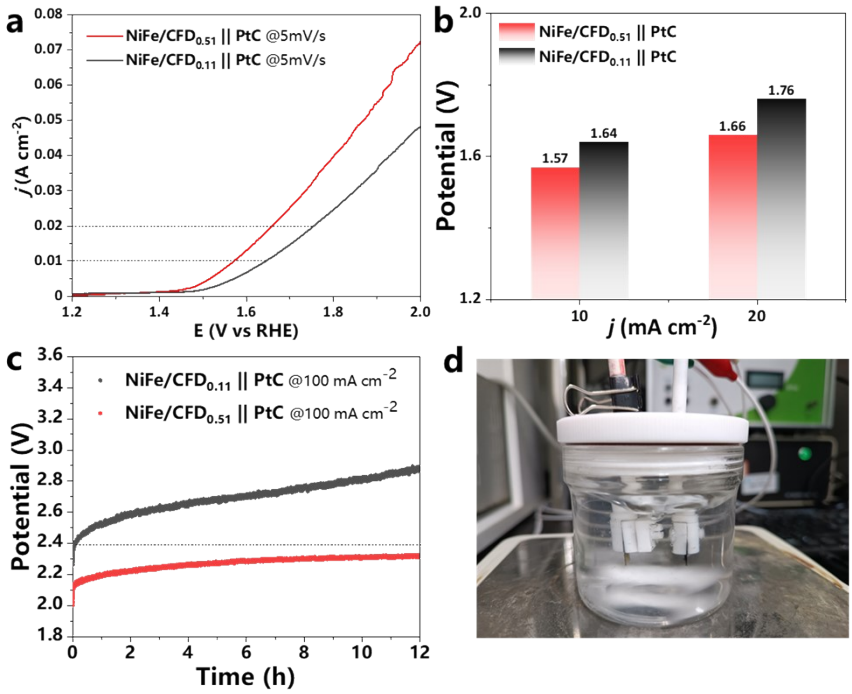

Figure S10. Comparison of the full water splitting in simulated seawater (1M KOH + 0.5M NaCl) using Pt/C as the cathodic electrocatalyst and the NiFe/$CFD_{0.11}$ or NiFe/$CFD_{0.51}$ as the anodic electrocatalysts: (a) the relevant two-electrode polarization curves and (b) comparison of full-cell potential under different current densities; (c) the galvanostatic profiles; (d) digital photo of the two-electrode cell for full water splitting.

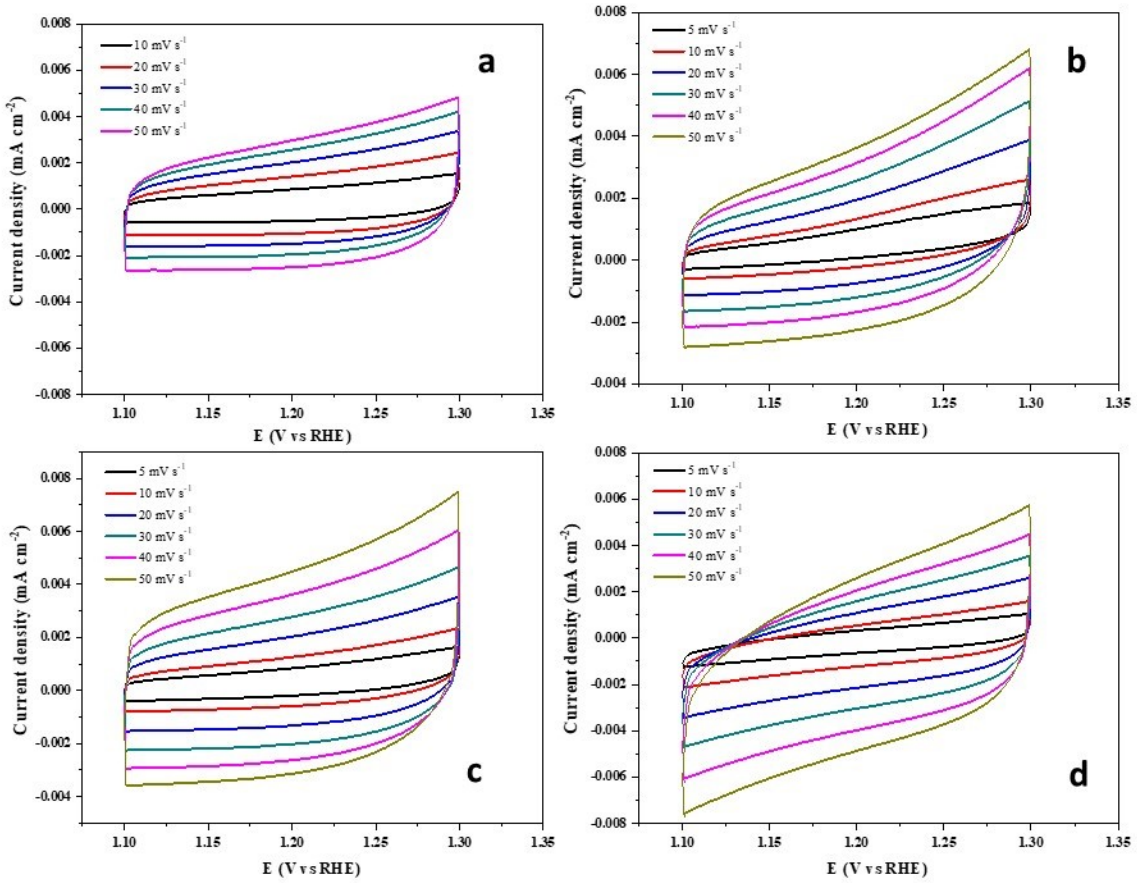

Figure S11. Cyclic voltammograms of (a) NiFe/$CFD_{0.11}$, (b) NiFe/$CFD_{0.26}$, (c) NiFe/$CFD_{0.41}$, (d) NiFe/$CFD_{0.51}$ electrocatalysts in the region of 0.1 - 0.3 V vs RHE in 1 M KOH.

References

[1] W. Ma, R. Ma, C. Wang, J. Liang, X. Liu, K. Zhou, T. Sasaki, A Superlattice of Alternately Stacked Ni-Fe Hydroxide Nanosheets and Graphene for Efficient Splitting ofWater, ACS Nano. 9 (2015) 1977–1984.

[2] J. Li, Z. Xia, X. Zhou, Y. Qin, Y. Ma, Y. Qu, Quaternary pyrite-structured nickel/cobalt phosphosulfide nanowires on carbon cloth as efficient and robust electrodes for water electrolysis, Nano Res. 10 (2017) 814–825.

[3] X. Han, C. Yu, Y. Niu, Z. Wang, Y. Kang, Y. Ren, H. Wang, H.S. Park, J. Qiu, Full Bulk-Structure Reconstruction into Amorphorized Cobalt–Iron Oxyhydroxide Nanosheet Electrocatalysts for Greatly Improved Electrocatalytic Activity, Small Methods. 4 (2020) 1–10.

[4] Y. Zheng, L. Zhang, H. Huang, F. Wang, L. Yin, H. Jiang, D. Wang, J. Yang, G. Zuo, ZIF-67-derived Co, Ni and S co-doped N-enriched porous carbon polyhedron as an efficient electrocatalyst for oxygen evolution reaction (OER), Int. J. Hydrogen Energy. 44 (2019)

27465–27471.

[5] H. Zhong, X. Cheng, H. Xu, L. Li, D. Li, P. Tang, N. Alonso-Vante, Y. Feng, Carbon fiber paper supported interlayer space enlarged Ni2Fe-LDHs improved OER electrocatalytic activity, Electrochim. Acta. 258 (2017) 554–560.

[6] K. Prabakaran, S.B. Ingavale, B. Kakade, Three dimensional NiS2–Ni(OH)2/CNT nanostructured assembly for supercapacitor and oxygen evolution reaction, J. Alloys Compd. 812 (2020) 152126.

[7] H.J. Song, H. Yoon, B. Ju, D.Y. Lee, D.W. Kim, Electrocatalytic Selective Oxygen Evolution of Carbon-Coated Na2Co1-xFexP2O7 Nanoparticles for Alkaline Seawater Electrolysis, ACS Catal. 10 (2020) 702–709.

[8] Q. Wang, L. Shang, R. Shi, X. Zhang, Y. Zhao, G.I.N. Waterhouse, L.Z. Wu, C.H. Tung, T. Zhang, NiFe Layered Double Hydroxide Nanoparticles on Co,N-Codoped Carbon Nanoframes as Efficient Bifunctional Catalysts for Rechargeable Zinc–Air Batteries, Adv. Energy Mater. 7 (2017) 1700467.

[9] S. Sekar, D.Y. Kim, S. Lee, Excellent Oxygen Evolution Reaction of Activated Carbon-Anchored NiO Nanotablets Prepared by Green Routes, Nanomaterials. 10 (2020) 1–13.

[10] V.C. Hoang, K.N. Dinh, V.G. Gomes, Hybrid Ni/NiO composite with N-doped activated carbon from waste cauliflower leaves: A sustainable bifunctional electrocatalyst for efficient water splitting, Carbon N. Y. 157 (2020) 515–524.

[11] S.H. Hsu, J. Miao, L. Zhang, J. Gao, H. Wang, H. Tao, S.F. Hung, A. Vasileff, S.Z. Qiao, B. Liu, An Earth-Abundant Catalyst-Based Seawater Photoelectrolysis System with 17.9% Solar-to-Hydrogen Efficiency, Adv. Mater. 30 (2018) 1–8.